Spin distributions and cross sections of evaporation residues in the ^{28}Si + ^{176}Yb reaction

K. Sudarshan,[1] R. Tripathi,[1,*] S. Sodaye,[1] S. K. Sharma,[1] P. K. Pujari,[1] J. Gehlot,[2] N. Madhavan,[2] S. Nath,[2] G. Mohanto,[2,†] I. Mukul,[2] A. Jhingan,[2] and I. Mazumdar[3]

[1]*Radiochemistry Division, Bhabha Atomic Research Centre, Mumbai-400 085, India*

[2]*Inter University Accelerator Centre, New Delhi-110 067, India*

[3]*Department of Nuclear and Atomic Physics, Tata Institute of Fundamental Research, Mumbai-400 005, India*

(Received 17 May 2016; revised manuscript received 23 December 2016; published 9 February 2017)

Background: Non-compound-nucleus fission in the preactinide region has been an active area of investigation in the recent past. Based on the measurements of fission-fragment mass distributions in the fission of ^{202}Po, populated by reactions with varying entrance channel mass asymmetry, the onset of non-compound-nucleus fission was proposed to be around $Z_pZ_t \sim 1000$ [Phys. Rev. C **77**, 024606 (2008)], where Z_p and Z_t are the projectile and target proton numbers, respectively.

Purpose: The present paper is aimed at the measurement of cross sections and spin distributions of evaporation residues in the ^{28}Si + ^{176}Yb reaction ($Z_pZ_t = 980$) to investigate the fusion hindrance which, in turn, would give information about the contribution from non-compound-nucleus fission in this reaction.

Method: Evaporation-residue cross sections were measured in the beam energy range of 129–166 MeV using the hybrid recoil mass analyzer (HYRA) operated in the gas-filled mode. Evaporation-residue cross sections were also measured by the recoil catcher technique followed by off-line γ-ray spectrometry at few intermediate energies. γ-ray multiplicities of evaporation residues were measured to infer about their spin distribution. The measurements were carried out using NaI(Tl) detector-based 4π-spin spectrometer from the Tata Institute of Fundamental Research, Mumbai, coupled to the HYRA.

Results: Evaporation-residue cross sections were significantly lower compared to those calculated using the statistical model code PACE2 [Phys. Rev. C **21**, 230 (1980)] with the coupled-channel fusion model code CCFUS [Comput. Phys. Commun. **46**, 187 (1987)] at beam energies close to the entrance channel Coulomb barrier. At higher beam energies, experimental cross sections were close to those predicted by the model. Average γ-ray multiplicities or angular momentum values of evaporation residues were in agreement with the calculations of the code CCFUS + PACE2 within the experimental uncertainties at all the beam energies.

Conclusions: Deviation of evaporation-residue cross sections from the "fusion + statistical model" predictions at beam energies close to the entrance channel Coulomb barrier indicates fusion hindrance at these beam energies which would lead to non-compound-nucleus fission. However, reasonable agreement of average angular momentum values of evaporation residues at these beam energies with those calculated using the coupled-channel fusion model with the statistical model codes CCFUS + PACE2 suggests that fusion suppression at beam energies close to the entrance channel Coulomb barrier where populated l waves are low is not l dependent.

DOI: 10.1103/PhysRevC.95.024604

I. INTRODUCTION

Investigation of fusion hindrance in reaction systems with low Z_pZ_t (Z_p, Z_t are projectile and target atomic numbers, respectively) has been an active area of investigation in the past decade. Due to the fusion hindrance, formation of evaporation residues is suppressed compared to the prediction of the statistical model describing the deexcitation of a fully equilibrated compound nucleus. Collision trajectories for which fusion is hindered may lead to non-compound-nucleus (NCN) fission resulting in anomalous fission-fragment angular distributions and/or broadening in the fission-fragment mass distributions. Therefore, evaporation-residue (ER) cross sections and fission-fragment mass and angular distributions have been studied extensively to investigate the entrance channel dynamics. For systems with low Z_pZ_t, particularly those forming compound nuclei (CN) in the preactinide region, results from different studies have not been conclusive. Based on the measurements of evaporation-residue cross sections and fission-fragment mass distributions, fusion suppression was reported in the ^{19}F + ^{197}Au and ^{30}Si + ^{176}Hf reactions [1]. However, fission-fragment angular distributions for ^{19}F + ^{197}Au [2] and ^{24}Mg + ^{192}Os [3] were observed to be in agreement with the predictions of the statistical saddle-point model (SSPM) [4,5] and, therefore, did not confirm the observed fusion hindrance in the ^{19}F + ^{197}Au reaction in Ref. [1]. Similarly, based on the measurements of fission-fragment mass distributions in the ^{16}O + ^{194}Pt and ^{24}Mg + ^{186}Pt reactions, Prasad *et al.* [6] reported a contribution from NCN fission in the ^{24}Mg + ^{186}Pt reaction, reflected as broader mass distributions compared to that in the ^{16}O + ^{194}Pt reaction. Whereas, Appannababu *et al.* [7] did not observe any broadening in the mass distributions in the ^{27}Al + ^{186}W

*Corresponding author: rahult@barc.gov.in

†Present address: Nuclear Physics Division, Bhabha Atomic Research Centre, Mumbai-400 085, India.

reaction compared to that in the $^{16}O + ^{197}Au$ reaction indicating an absence of any contribution from NCN fission. On the other hand, results of different studies for reaction systems with large entrance channel Coulomb repulsion have been observed to be mutually consistent. Sagaidak *et al.* [8] observed a substantial reduction in the formation of evaporation residues in the $^{48}Ca + ^{168,170}Er$ ($Z_pZ_t = 1360$). Similarly, Chizhov *et al.* [9] observed an asymmetric component in the mass distributions in the $^{48}Ca + ^{168}Er$ reaction, which was attributed to the contribution from NCN fission. Trotta *et al.* [10] reported suppression in evaporation-residue formation and anomalous fission-fragment angular distributions in the $^{48}Ca + ^{154}Sm$ reaction. Due to the contribution from NCN fission, fission-fragment angular distributions showed a forward-backward asymmetry [10].

Although the results from various observables for systems with large Z_pZ_t appear to be consistent, for systems with low Z_pZ_t, more studies are required to understand the phenomenon of fusion hindrance. Rafiei *et al.* [11] measured fission-fragment mass distributions in the fission of ^{202}Po populated by reactions involving different entrance channel mass asymmetry values. Based on these studies, the onset of NCN fission was proposed to be around $Z_pZ_t \sim 1000$. A study of fission-fragment angular distributions in the $^{28}Si + ^{176}Yb$ ($Z_pZ_t = 980$) reaction forming a similar compound nucleus (^{204}Po) did not show any large contribution from NCN fission as angular anisotropies were close to that predicted by SSPM [12]. However, it should be mentioned here that, in the preactinide region, i.e., in the less fissile systems, sensitivity of the fission-fragment angular distributions to the contribution from NCN fission is reduced as angular anisotropy becomes high even for CN fission and the difference in angular anisotropy for CN and NCN fission decreases. This is due to the fact that fission mainly results from higher l waves. In this mass region, evaporation residues would be a better probe to investigate the fusion hindrance. In the case of fusion hindrance, evaporation-residue cross sections would be suppressed compared to the prediction of statistical theory for compound-nucleus deexcitation. It has been shown that the spin distributions of evaporation residues also can provide information about the fusion hindrance which decreases average angular momentum of ERs as higher l waves preferentially undergo NCN fission [13–15]. Thus the reduction in the compound-nucleus formation probability may be due to the large entrance channel Coulomb repulsion, reduction in the fission barrier, or for collision trajectories with higher l values.

In the present work, cross sections and spin distributions of ERs have been measured in the beam energy range of 129.4–165.8 MeV corresponding to the $E_{\mathrm{c.m.}}/V_{\mathrm{b}}$ ($E_{\mathrm{c.m.}}$ and V_{b}, respectively, are the available energy and entrance channel Coulomb barrier in the center-of-mass frame of reference) values of 0.98–1.26, respectively, to investigate the fusion hindrance in this reaction. The results have been compared with the theoretical calculations based on the statistical model code PACE2 [16] with fusion cross sections calculated from coupled-channel fusion model code CCFUS [17] as input.

II. EXPERIMENTAL DETAILS

Evaporation-residue cross sections and γ-ray multiplicities were measured in $^{28}Si + ^{176}Yb$ reaction using the hybrid recoil mass analyzer (HYRA) operated in the gas-filled mode coupled to the Tata Institute of Fundamental Research (TIFR) 4π-spin spectrometer [18,19] at the 15UD Pelletron-LINAC Accelerator Facility at the Inter University Accelerator Centre (IUAC), New Delhi. The off-line measurement of cross sections of evaporation residues using the recoil catcher technique was carried out at the BARC-TIFR Pelletron-LINAC Facility, Mumbai. For on-line measurements at IUAC, an electrodeposited target of ^{176}Yb of thickness $\sim 150\,\mu g/cm^2$ on a thin aluminum ($540\,\mu g/cm^2$) backing of 9-mm diameter was used for the experiments. The experiments were carried out with ^{28}Si beam of energy of 143–178 MeV (in steps of 7 MeV) provided by the accelerator facility after the energy boost by LINAC. The corresponding mean beam energies in the target were 129.4–165.8 MeV after the energy degradation in the nickel foil (isolating the accelerator vacuum from the gas-filled separator) at the entrance of the target chamber and aluminum backing of the target facing the beam. A fixed tantalum collimator was used before the entrance window foil to minimize the beam spot size. In the subsequent part of the paper, only beam energies after the degradation are mentioned. ERs were separated from the beam particles by the HYRA, operated in a gas-filled mode and detected by a multiwire proportional counter (MWPC) at the focal plane. In order to normalize for the target thickness and beam intensity, elastically scattered beamlike particles were detected using two monitor detectors placed at $\pm 25^\circ$. For a clear selection of evaporation residues, the time of flight (TOF) of the ERs with respect to the beam pulse as well as the energy loss signal from the MWPC were recorded.

In order to determine the residue spin distributions, prompt yrast γ rays emitted by the residues were detected by a 4π-spin spectrometer consisting of 28 NaI(Tl) detectors [18,19] in soccer ball geometry. γ-ray fold distribution spectra were recorded as the number of NaI(Tl) detectors fired in the set time window for an accepted event. The spectrometer covered about 88% of the 4π geometry and ER-gated γ-ray fold data of up to $\sim$20 folds could be recorded. A typical set of singles and ER-gated γ-ray fold distribution spectra at the beam energy of 165.8 MeV are shown in Fig. 1. Fold distributions were gated with TOF and cathode (of the MWPC) signals to select the fold distribution of the evaporation residues. The TOF of the evaporation residues was recorded with respect to the beam pulse. The inset in Fig. 1 shows the counts corresponding to each fold with and without evaporation-residue gate. The raw data of fold distribution at lower folds had contamination from other sources, such as Coulomb excitation, fusion of ^{28}Si with an aluminum backing, γ rays from the tantalum collimator, as well as from the entrance window foil. The low fold contamination was suppressed by orders of magnitude by using the 'OR' gate output of signals from focal plane of the MWPC and monitor detectors as a strobe while acquiring the fold distribution spectra. The contamination was further suppressed by an order of magnitude when the spectra were taken in coincidence with the ERs as seen from the large

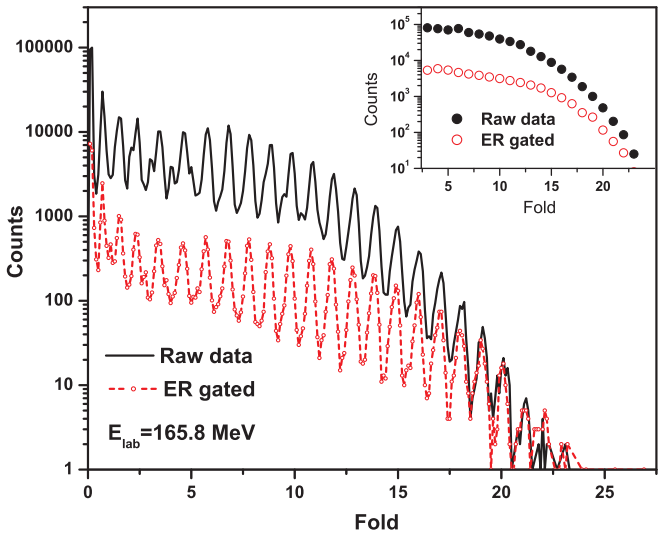

FIG. 1. Singles and evaporation-residue-gated γ-ray fold distribution spectra in the ^{28}Si + ^{176}Yb reaction at E_{lab} of 165.8 MeV. The inset shows the counts in each fold.

reduction in the counts in lower folds in the gated spectrum. For the lower folds (<3), some contamination would still be present, and therefore they were not included in the fitting.

For off-line measurements, ^{176}Yb targets of $\sim$300 μg/cm^2 electrodeposited on aluminum foil of thickness 2.5 mg/cm^2 were irradiated with a ^{28}Si beam of 138–154 MeV for 2 to 3 h with ^{176}Yb layer facing the beam at the BARC-TIFR Pelletron-LINAC Facility. The beam current was $\sim$30–40 enA during the irradiation. A secondary electron suppressed Faraday cup was used to measure the integrated beam current for every 10-s interval to correct for the variations in the beam current during the irradiation. Evaporation residues were stopped in the aluminum backing and were assayed using off-line γ-ray spectrometry with a high-purity germanium (HPGe) detector. The activity was followed as a function of time to identify various evaporation residues by matching their characteristic γ-ray energies and half-lives. The decay data of ERs used in the present work are given in Table I. Standard ^{152}Eu^{g} and ^{133}Ba^{g} sources were used for the γ-ray detection efficiency calibration of the detector for the specific geometry used.

III. RESULTS AND DISCUSSION

A. Evaporation-residue cross sections

From the measured count rates of evaporation residues (N_{ER}) in the focal plane detector and elastically scattered beam particles (N_{mon}) in the monitor detectors, the evaporation-residue cross sections (σ_{ER}) were determined as

$$\sigma_{ER} = \frac{N_{ER}}{N_{mon}} \left(\frac{d\sigma}{d\Omega}\right)_{Ruth} \frac{\Delta\Omega_{mon}}{\varepsilon_{HYRA}}, \quad (1)$$

where $(\frac{d\sigma}{d\Omega})_{Ruth}$ is the differential Rutherford scattering cross section, $\Delta\Omega_{mon}$ is the solid angle subtended by the monitor detector, and ε_{HYRA} is the transmission efficiency of the HYRA for evaporation residues, i.e., ratio of the evaporation residues produced to those reaching the focal plane of the HYRA. The value of the monitor counts (N_{mon}) is taken as the geometric mean of the counts in the two monitor detectors placed at $\pm$25° with respect to the beam direction. In the beam energy range studied in the present work where ERs had sufficiently high energy due to charge state and energy focusing conditions with the optimized parameters, the variation in ε_{HYRA} with beam energy should be dependent only on the angular distribution of the evaporation residues. The fraction of evaporation residues falling in the acceptance angle ($\pm$3.4°) of the HYRA would vary depending on the angular distribution of the ERs. Transmission efficiency of the HYRA (ε_{HYRA}) was estimated based on ER cross sections in the reactions studied earlier using the HYRA setup [20,21], but no separate experiment to determine the efficiency for this system was carried out. Hence, the efficiency determined is a relative quantity as other experimental uncertainties, such as differences in the beam spot size on the target due to angular straggling in the entrance window and the effect of tantalum collimator, etc., could not be accounted for. However, such factors would be independent of beam energy but would only depend on the choice and thickness of the entrance window foil and the presence or absence of a tantalum collimator. The angular distribution of the ERs was calculated for the ^{31}P + ^{170}Er and

TABLE I. Half-life ($T_{1/2}$), γ-ray energy (E_γ), and abundance (a_γ) taken from Ref. [24] along with the formation cross sections of the evaporation residues formed in the ^{28}Si + ^{176}Yb reaction.

Nuclide	$T_{1/2}$ (min)	E_γ (keV)	a_γ (%)	Cross section (mb)			
				138 MeV	145 MeV	149 MeV	154 MeV
^{200}Po	11.5	671	34.0	17.4 ± 1.4	7.1 ± 1.2	6.0 ± 1.3	4.5 ± 1.3
^{200}B i^{m}	31	1026.5	91	3.8 ± 3	5.4 ± 1.3	2.7 ± 0.8	
		462.3	37.9				
^{199}P o^{m,a}		383.6	91	38.7 ± 5.4	54.8 ± 0.7	43.0 ± 1	30.1 ± 4
(^{195}Pb)	15						
^{199}Bi[a]		366.9	44.2	8.2 ± 2.6	8 ± 3		
(^{199}Pb)	90						
^{198}Po[a]		581.8	18.8		17.2 ± 1.1	27.8 ± 2.4	38.9 ± 1.1
(^{194}Pb)	12						

[a]Cross sections have been measured from the activity of the daughter as given inside the parentheses.

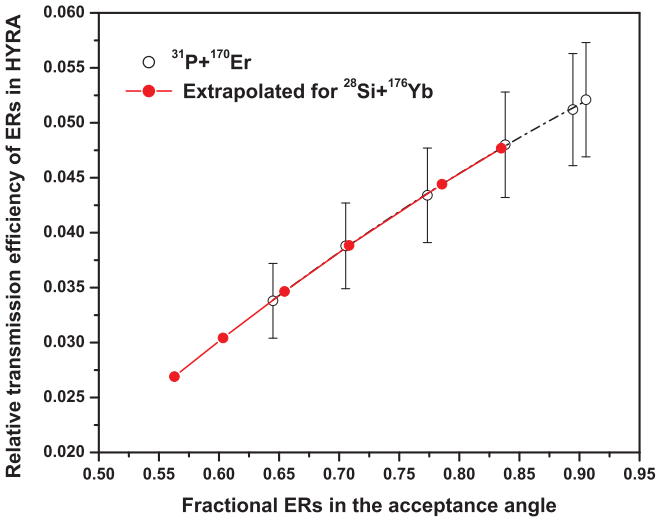

FIG. 2. Plot of relative transmission efficiency of the HYRA as a function of the fraction of ERs emitted in the acceptance angle of the HYRA. The relative transmission efficiency of the ERs in the ^{28}Si + ^{176}Yb reaction is deduced from earlier measurements in the ^{31}P + ^{170}Er system [22].

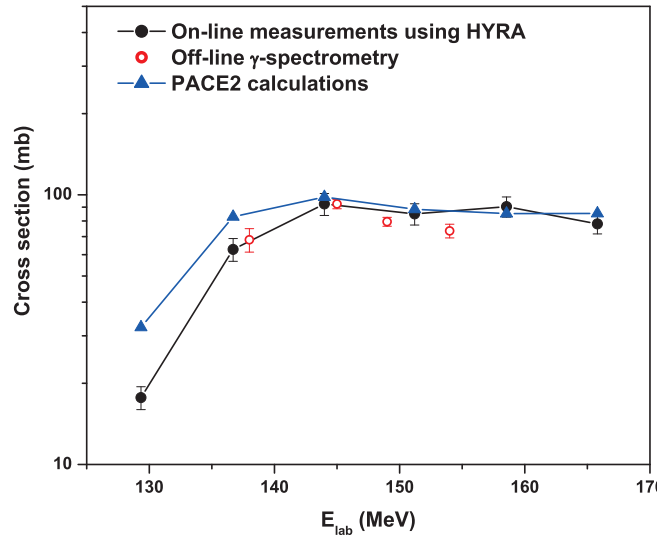

FIG. 3. Cross sections of evaporation residues in the ^{28}Si + ^{176}Yb reaction. The parameters for the PACE2 calculations were fixed by reproducing the fission cross section data for the ^{16}O + ^{188}Os reaction [12].

^{28}Si + ^{176}Yb reactions using codes CCFUS + PACE2 [16,17]. From the angular distributions of the ERs, fractions of ERs in the acceptance angle of the HYRA (±3.4°) in both reactions were calculated. By evaluating the fraction of the ERs in the acceptance angle with the transmission efficiency determined in previous experiments [20,21] the relative transmission efficiency for the present experiment is estimated and is shown in Fig. 2. Accordingly, the cross sections determined using Eq. (1) are relative and have been normalized to those from off-line measurements as discussed later.

In order to determine the production cross sections of the ERs by the off-line method, peak areas under their characteristic γ rays in the γ-ray spectrum were obtained using the peak area analysis software PHAST [23] which were used to obtain the activities of the ERs at the end of irradiation using the following equation:

$$A = \frac{P A \frac{CT}{LT}}{e^{-\lambda T_{\rm cool}}[(1 - e^{-\lambda CT})/\lambda] a_\gamma \varepsilon_\gamma}, \qquad (2)$$

where $T_{\rm cool}$ is the time elapsed between the end of irradiation and the starting of the γ-ray spectrum acquisition, LT and CT are the live time of the analog-to-digital converter in the counting system and the corresponding clock time, respectively. λ is the decay constant of the ER, and a_γ is the abundance of the γ ray in the decay of that particular ER. ε_γ is the full energy γ-ray detection efficiency of the HPGe detector for the energy of the γ ray under consideration. The nuclear decay data of the ERs (λ and a_γ) were taken from the Table of Isotopes [24] and are given in Table I. The first term in the denominator of Eq. (2) is a correction factor for the decay during cooling, whereas the second term is a correction for the decay during the spectrum acquisition time. From the activity at the end of irradiation (A), the production cross section (σ) of an ER was calculated as

$$\sigma = \frac{A}{N \sum_{i=1}^{n} \phi_i (1 - e^{-\lambda\, \Delta T_{\rm irr}}) e^{-\lambda (T_{\rm irr} - i\, \Delta T_{\rm irr})}}, \qquad (3)$$

where N is the number of target atoms/cm^2, n is the number of intervals in which the integrated beam current was recorded, ϕ_i is the beam intensity (beam flux) in the ith interval, $T_{\rm irr}$ is the irradiation time, and $\Delta T_{\rm irr}$ is the time interval (10 s) for recording the beam current. The number density of target atoms was measured by neutron activation analysis. For any ER which had a contribution from the decay of its parent, appropriate parent-daughter decay-growth equations were used to correct for the contribution of the parent's decay to the daughter's activity and to obtain direct production cross sections of the ER. Production cross sections of various evaporation residues are also given in Table I.

The total cross sections of ERs measured by the off-line method at different beam energies are shown in Fig. 3 as open circles. The on-line ER cross sections determined using the HYRA are shown in Fig. 3 as filled circles. The on-line ER cross sections were normalized with off-line values at $E_{\rm lab} = 145$ MeV. The ER cross sections calculated using the statistical model code PACE2 with CCFUS predicted fusion l distributions as input are also shown in the figure. For CCFUS calculations, deformation data of excited states of the projectile and target were taken from Ref. [25]. The parameters for the PACE2 calculations were fixed by reproducing the fission cross sections in the ^{16}O + ^{188}Os reaction, which forms the same compound nucleus, and as for this system, purely compound-nucleus fission is expected. The calculated cross sections (triangles) are close to the experimental cross sections at higher beam energies. Some of the possible ERs had nonsuitable nuclear characteristics for off-line γ-ray spectrometry. Based on PACE2 calculations, these ERs make up nearly 5%–10% of the total ER cross sections determined, thus experimental ER

cross sections measured by the recoil catcher technique may be underestimated at most by ∼10%. At higher beam energies, a small contribution from non-compound-nucleus fission may be present arising from the large l waves, which would reduce the fission barrier. However, it is not possible to conclude about the contribution from NCN fission at higher beam energies due to their small magnitude and large uncertainties associated with calculations and experimental data. It can be seen from the figure that the experimental cross sections are significantly lower compared to the values calculated using the codes CCFUS + PACE2 at the lowest two beam energies which are close to the entrance channel Coulomb barrier. In Ref. [26], the authors have compared experimental ER cross section data of a large number of systems with their statistical model calculations. According to their calculations, a substantial suppression has been observed in the present reaction for all the beam energies. In our calculations using the statistical model codes CCFUS + PACE2 with the parameters fixed by reproducing the experimental fission cross section data of the ^{16}O + ^{188}Os system [12], a clear suppression is observed only at lower beam energies. The deviation in ER cross sections increases from 18% ± 2% at $E_{\rm lab} = 136.7$ MeV ($E_{\rm c.m.}/V_{\rm b} = 1.04$) to 41% ± 4% at $E_{\rm lab} = 129.4$ MeV ($E_{\rm c.m.}/V_{\rm b} = 0.98$). The absolute estimate of fusion suppression may vary due to the uncertainty of the theoretical calculations. In the theoretical calculations, the ER cross section can be lowered to match the experimental value by increasing the fission competition (in PACE2 calculations), by lowering the fusion cross section (in CCFUS calculations), or a combination of both. However, increasing the fission competition to reproduce the ER cross section at the lowest beam energy resulted in a large underestimation of the ER cross sections at higher beam energies. Whereas, decreasing the fusion cross section significantly underestimated the experimental fission cross sections reported in Ref. [27]. Thus, the experimental ER cross sections in the ^{28}Si + ^{176}Yb reaction cannot be explained by varying the model parameters. In the measurements by Rafiei *et al.* [11], an enhancement in the deviation of the variance of mass distribution from that expected for compound-nucleus fission can be seen as the beam energy goes down through the entrance channel Coulomb barrier for the ^{34}S + ^{168}Er ($Z_pZ_t = 1088$) and ^{48}Ti + ^{154}Sm ($Z_pZ_t = 1364$) reactions, although the magnitude of deviation decreases with decreasing Z_pZ_t. Thus, the observed suppression of the ER cross sections in the present paper ($Z_pZ_t = 980$) is consistent with the observation of the contribution of the non-compound-nucleus fission in the ^{34}S + ^{168}Er and ^{48}Ti + ^{154}Sm reactions. The suppression in the ER cross sections and broadening in the fission-fragment mass distributions [11] near the entrance channel Coulomb barrier indicates the contribution from quasifission, which may be due to target deformation.

B. Spin distributions of evaporation residues

The experimentally measured γ-ray fold distributions were fitted using the formalism described by Van Der Werf [28]. According to this formalism, the probability of detecting the l number of γ rays (l-fold detection probability or l number of detectors fired) when the spectrometer consists of N number of detectors and if M-uncorrelated γ rays are emitted within the time window is given by

$$P^{M}_{N,l}(\varepsilon_1,\varepsilon_2,\ldots,\varepsilon_N) = \sum_{i=0}^{l}(-1)^{l-i}\binom{N-i}{N-l} \times\left\{\sum_{l_a(i)}\left[1-\left(\sum_{j=1}^{N}\varepsilon_j-\sum_{k=1}^{i}\varepsilon_{a\,k}\right)^{M}\right]\right\}, \quad (4)$$

where $\binom{N-i}{N-l}$ represents all combinations in which $N-l$ can be taken out of $N-i$ and $\Sigma_{l_a(i)}$ represents the summation over all possible permutations in which i can be taken out of N, ε_i is the γ-ray detection efficiency of the detector. Using a FORTRAN program, varying the number of γ rays emitted, i.e., multiplicity M (M = 1–50), the probability of detection of the l number of γ rays for each M ($l = 1$ to M) was calculated according to Eq. (4). The efficiency of each detector was estimated using a standard source of ^{137}Cs at the target position. The multiplicity distribution or probability of emission of M γ rays [$P(M)$] was assumed to have the shape of a modified Fermi function [15,29,30],

$$P(M) = \frac{(2M+1)}{1+\exp\left(\frac{M-M_0}{\Delta M}\right)}, \quad (5)$$

with M_0 and ΔM as variable parameters. With an assumed multiplicity distribution, the fold distribution is calculated as

$$p(m) = \sum_{M=m}^{\infty} P^{M}_{N,m}(\varepsilon_1,\varepsilon_2,\ldots,\varepsilon_N)P(M). \quad (6)$$

Experimental fold distribution was fitted using Eq. (6) with relevant quantities calculated using Eqs. (4) and (5). In the fitting process, M_0 and ΔM were kept as free parameters. A typical fitting of the fold distribution for $E_{\rm lab} = 144$ MeV is shown in Fig. 4(a).

The γ rays involved in the deexcitation of evaporation residues have energy distributions, although most of them are below 1 MeV. In order to estimate the uncertainty on the evaluated multiplicity, arising due to the use of single efficiency value corresponding to 662 keV for all the γ rays, multiplicity distributions also were calculated assuming the efficiency of detection to be ±10% compared to that estimated for 662 keV. As expected, the average multiplicity extracted would be lower or higher depending on whether the assumed efficiency is higher or lower compared with the experimental efficiency. Three multiplicity distributions extracted assuming different average γ-ray detection efficiencies for $E_{\rm lab} = 144$ MeV are shown in Fig. 4(b). The average of these three multiplicity distributions is taken as the experimental multiplicity distribution as shown in Fig. 4(c). The uncertainty quoted on the mean multiplicity is the difference in the extracted multiplicity assuming that the actual energy averaged detection efficiency can differ from that estimated using 662 keV by ±10%. A similar procedure is adopted for extracting multiplicity distributions at other beam energies. The extracted multiplicity distributions are shown in Fig. 5. It is seen that the multiplicity distributions become broader with

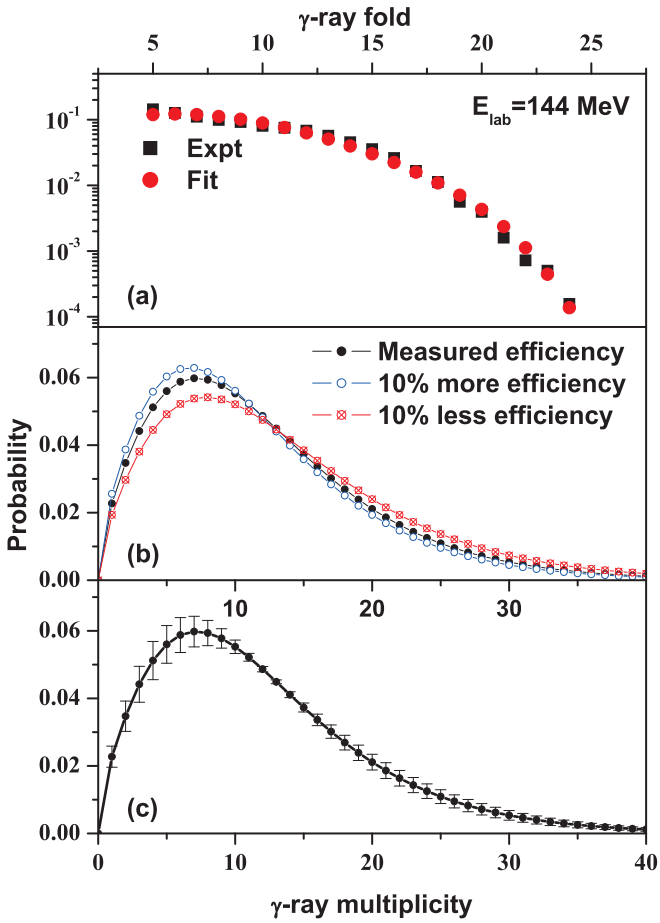

FIG. 4. (a) Typical fitting of the experimental fold distribution (x-axis scale on the top) data at $E_{\rm lab} = 144$ MeV. (b) Multiplicity distributions obtained using the γ-ray detection efficiency as measured at 662 keV and by varying the efficiency by $\pm 10\%$ compared to that measured at 662 keV. (c) Average multiplicity distribution.

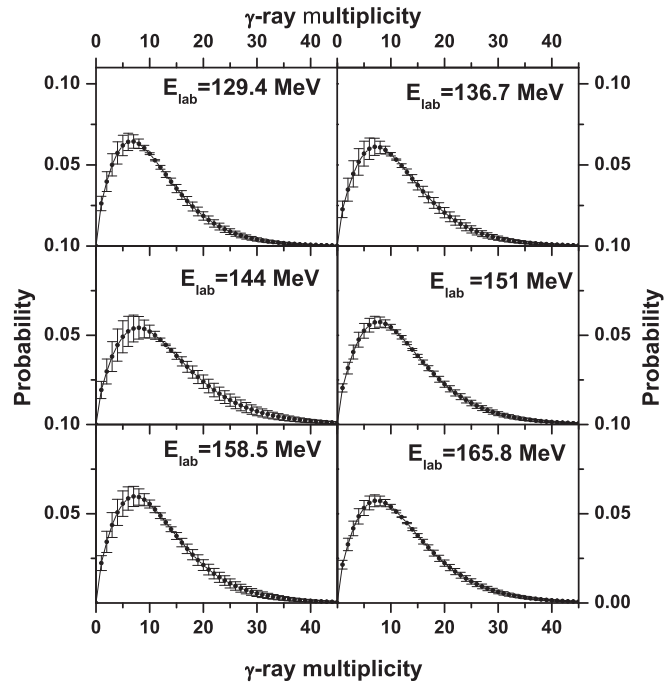

FIG. 5. γ-ray multiplicity distributions extracted from the measured fold distributions in coincidence with evaporation residues in the reaction of ^{28}Si + ^{176}Yb.

maxima marginally shifting to higher values with an increase in the beam energy. For evaluating the l distribution of the ERs, the measured multiplicity distributions can be converted to spin distributions of the ERs by taking the average angular momentum carried by each γ ray to be constant. The major ERs are $^{198-200}$Po, $^{199-200}$Bi, and $^{196-197}$Pb in the beam energy range of the present work. The level schemes of the ERs [31] show that the γ-ray transitions involved are of mainly the $E2$, $M1$, and $E1$ types and the energy of the γ rays is in the range of 100 keV to 3 MeV. In a model where one has $E1$ emissions to get down to the yrast line and then stretched $E2$ transitions to get to the ground state, there would be relatively more $E1$ at low spins, and the average angular momentum carried would be smaller. Similarly, at higher spins where the difference between the excitation energy and the energy of the yrast line is much less than the average binding energy of a nucleon, statistical $E1$ emission is more probable to reach the yrast line than particle evaporation. Hence, calculated average γ-ray multiplicities using the statistical model code PACE2 with fusion l distribution from CCFUS as the input are directly compared with experimental multiplicities and are shown in Fig. 6.

In the measurement of γ-ray multiplicities, some of the γ rays are converted giving low-energy x rays and are, therefore, not registered. Hence, the predicted γ multiplicities have to be corrected for conversion for comparing with the measured γ-ray multiplicities of ERs. The internal conversion coefficients were calculated in the energy range of 100 keV to 3 MeV in

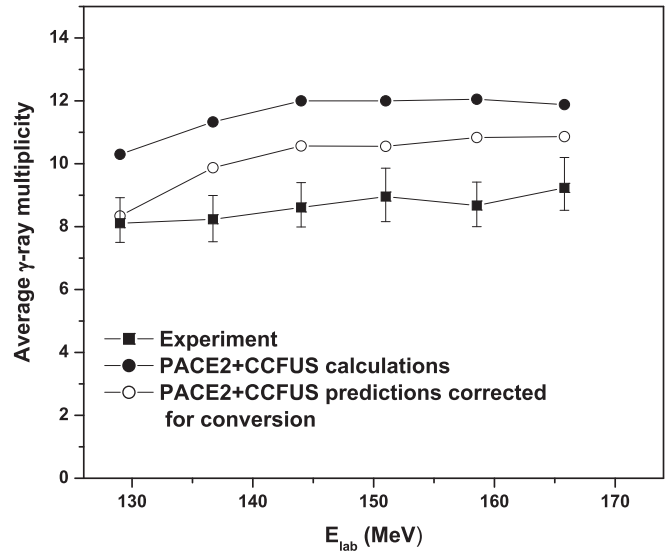

FIG. 6. The average γ-ray multiplicities of the evaporation residues in the ^{28}Si + ^{176}Yb reaction as a function of beam energy. The average γ-ray multiplicities predicted from the statistical model code PACE2 [16] with fusion l distribution calculated using the code CCFUS [17] also are given for comparison.

the system of $Z = 84$ for transitions of various multipolarities [32]. Based on the internal conversion coefficients, it is estimated that on average nearly 10%–20% of the γ rays are converted. The number of γ rays lost due to conversion is calculated at and is subtracted from predicted multiplicities. The average γ-ray multiplicities after correcting for the conversion are also given in Fig. 6.

It can be seen from Fig. 6 that the experimental values of average multiplicities are close to the statistical model predictions. Although, it was observed that the ER cross sections were suppressed at the energies close to the entrance channel Coulomb barrier (Fig. 3), it is not reflected in the γ-ray multiplicities or spin distributions of the evaporation residues. The effect of the contribution from NCN fission on $\langle l \rangle$ may be observed with heavier projectiles and at higher beam energies which populate large l waves. The resultant substantial reduction in the fission barrier may allow the heavy dinuclear system to fission without being captured inside the saddle point.

IV. CONCLUSIONS

Cross sections and spin distributions of evaporation residues were measured in the ^{28}Si + ^{176}Yb reaction, which lies close to the proposed onset ($Z_p Z_t \sim 1000$) of fusion hindrance [11]. It was observed that the evaporation-residue cross sections are close to values calculated using the statistical model code CCFUS + PACE2 at higher beam energies. However, at beam energies close to the entrance channel Coulomb barrier, experimental values are significantly lower compared to the calculated values with the difference being more pronounced at the lowest beam energy. Observation of fusion suppression at beam energies close to the entrance channel Coulomb barrier is consistent with the observation of the contribution from non-compound-nucleus fission based on the broadening of the mass distributions in Ref. [11] for similar systems at near- and sub-barrier energies and due to the target deformation effect.

Average γ-ray multiplicities of the evaporation residues were in reasonable agreement with those calculated using the statistical model code PACE2 with fusion input from CCFUS, even at the lower beam energies for which experimental cross sections were lower compared to the PACE2 values. This is due to the fact that the l waves populated close to the entrance channel Coulomb barrier are not large enough to cause a substantial reduction in the fission barrier, the lowering of which may lead to a large contribution from non-compound-nucleus fission and, thus, hindrance to fusion. Such effects are expected to be pronounced with heavier projectiles at higher beam energies.

[1] A. C. Berriman, D. J. Hinde, M. Dasgupta, C. R. Morton, R. D. Butt, and J. O. Newton, Nature (London) **413**, 144 (2001).

[2] R. Tripathi, K. Sudarshan, S. Sodaye, A.V. R. Reddy, K. Mahata, and A. Goswami, Phys. Rev. C **71**, 044616 (2005).

[3] R. Tripathi, K. Sudarshan, S. Sodaye, K. Mahata, A. Goswami, and A.V. R. Reddy, Int. J. Mod. Phys. E **17**, 419 (2008).

[4] R. Vandenbosch and J. R. Huizenga, *Nuclear Fission* (Academic, London, 1973).

[5] I. Halpern and V. M. Strutinsky, in *Proceedings of the Second United Nations International Conference on Peaceful Uses of Atomic Energy, Geneva, 1958*, edited by J. H. Martens *et al.* (United Nations, Switzerland, 1958), Vol. 15, p. 408.

[6] E. Prasad, K. M. Varier, R. G. Thomas, P. Sugathan, A. Jhingan, N. Madhavan, B. R. S. Babu, R. Sandal, S. Kalkal, S. Appannababu, J. Gehlot, K. S. Golda, S. Nath, A. M. Vinodkumar, B. P. A. Kumar, B. V. John, G. Mohanto, M. M. Musthafa, R. Singh, A. K. Sinha, and S. Kailas, Phys. Rev. C **81**, 054608 (2010).

[7] S. Appannababu, S. Mukherjee, B. K. Nayak, R. G. Thomas, P. Sugathan, A. Jhingan, E. Prasad, D. Negi, N. N. Deshmukh, P. K. Rath, N. L. Singh, and R. K. Choudhury, Phys. Rev. C **83**, 034605 (2011).

[8] R. N. Sagaidak, G. N. Kniajeva, I. M. Itkis, M. G. Itkis, N. A. Kondratiev, E. M. Kozulin, I. V. Pokrovsky, A. I. Svirikhin, V. M. Voskressensky, A. V. Yeremin, L. Corradi, A. Gadea, A. Latina, A. M. Stefanini, S. Szilner, M. Trotta, A. M. Vinodkumar, S. Beghini, G. Montagnoli, F. Scarlassara, D. Ackermann, F. Hanappe, N. Rowley, and L. Stuttgé, Phys. Rev. C **68**, 014603 (2003).

[9] A. Yu. Chizhov, M. G. Itkis, I. M. Itkis, G. N. Kniajeva, E. M. Kozulin, N. A. Kondratiev, I. V. Pokrovsky, R. N. Sagaidak, V. M. Voskressensky, A. V. Yeremin, L. Corradi, A. Gadea, A. Latina, A. M. Stefanini, S. Szilner, M. Trotta, A. M. Vinodkumar, S. Beghini, G. Montagnoli, F. Scarlassara, A. Y. Rusanov, F. Hanappe, O. Dorvaux, N. Rowley, and L. Stuttgé, Phys. Rev. C **67**, 011603 (2003).

[10] M. Trotta, A. M. Stefanini, B. R. Behera, L. Corradi, E. Fioretto, A. Gadea, S. Szilner, Y. W. Wu, S. Beghini, G. Montagnoli, F. Scarlassara, A. Yu. Chizhov, I. M. Itkis, G. N. Kniajeva, N. A. Kondratiev, E. M. Kozulin, I. V. Pokrovsky, R. N. Sagaidak, V. M. Voskressensky, F. Haas, and N. Rowley, Prog. Theor. Phys. Suppl. **154**, 37 (2004).

[11] R. Rafiei, R. G. Thomas, D. J. Hinde, M. Dasgupta, C. R. Morton, L. R. Gasques, M. L. Brown, and M. D. Rodriguez, Phys. Rev. C **77**, 024606 (2008).

[12] R. Tripathi, K. Sudarshan, S. K. Sharma, K. Ramachandran, A. V. R. Reddy, P. K. Pujari and A. Goswami, Phys. Rev. C **79**, 064607 (2009).

[13] P. D. Shidling, N. Madhavan, V. S. Ramamurthy, S. Nath, N. M. Badiger, S. Pal, A. K. Sinha, A. Jhingan, S. Muralithar, P. Sugathan, S. Kailas, B. R. Behera, R. Singh, K. M. Varier, and M. C. Radhakrishna, Phys. Lett. B **670**, 99 (2008).

[14] G. Mohanto, N. Madhavan, S. Nath, J. Sadhukhan, J. Gehlot, I. Mazumdar, M. B. Naik, E. Prasad, I. Mukul, T. Varughese, A. Jhingan, R. K. Bhowmik, A. K. Sinha, D. A. Gothe, P. B. Chavan, S. Pal, V. S. Ramamurthy, and A. Roy, Nucl. Phys. A **890-891**, 62 (2012).

[15] S. K. Hui, C. R. Bhuinya, A. K. Ganguly, N. Madhavan, J. J. Das, P. Sugathan, D. O. Kataria, S. Mutlithar, L. T. Baby, V. Tripathi, A. Jhingan, A. K. Sinha, P. V. M. Rao, N. V. S. V. Prasad, A. M. Vinodkumar, R. Singh, M. Thoennessen, and G. Gervais, Phys. Rev. C **62**, 054604 (2000).

[16] A. Gavron, Phys. Rev. C **21**, 230 (1980).

[17] C. H. Dasso and S. Landowne, Comput. Phys. Commun. **46**, 187 (1987).
[18] N. Madhavan, I. Mazumdar, T. Varughese, J. Gehlot, S. Nath, D. A. Gothe, P. B. Chavan, G. Mohanto, M. B. Naik, I. Mukul, and A. K. Sinha, EPJ Web Conf. **17**, 14003 (2011).
[19] G. A. Kumar, I. Mazumdar, and D. A. Gothe, Nucl. Instrum. Methods Phys. Res., Sect. A **611**, 76 (2009).
[20] E. Prasad, K. M. Varier, N. Madhavan, S. Nath, J. Gehlot, S. Kalkal, J. Sadhukhan, G. Mohanto, P. Sugathan, A. Jhingan, B. R. S. Babu, T. Varughese, K. S. Golda, B. P. A. Kumar, B. Satheesh, S. Pal, R. Singh, A. K. Sinha, and S. Kailas, Phys. Rev. C **84**, 064606 (2011).
[21] G. Mohanto, N. Madhavan, S. Nath, J. Gehlot, I. Mukul, A. Jhingan, T. Varughese, A. Roy, R. K. Bhowmik, I. Mazumdar, D. A. Gothe, P. B. Chavan, J. Sadhukhan, S. Pal, M. Kaur, V. Singh, A. K. Sinha, and V. S. Ramamurthy, Phys. Rev. C **88**, 034606 (2013).
[22] G. Mohanto, Ph.D. thesis, Inter University Accelerator Centre, New Delhi, India, 2013.
[23] P. K. Mukhopadhyaya, in *Proceedings of DAE Symposium on Intelligent Nuclear Instrumentation (INIT-2001)*, edited by S. K. Kataria, P. P. Vaidya, P. V. Narurkar, and S. Roy (BARC, Mumbai, India, 2001), p. 307.
[24] R. B. Firestone and V. S. Shirley, *Table of Isotopes*, 8th ed. (Wiley-Interscience, New York, 1999).
[25] S. Raman, C. W. Nestor, and P. Tikkanen, At. Data Nucl. Data Tables **78**. 1 (2001); T. Kibedi and R. H. Spear, *ibid.* **80**, 35 (2002); JENDL 3.2; available online at https://www-nds.iaea.org/RIPL-2/
[26] T. Banerjee, S. Nath, and S. Pal, Phys. Rev. C **91**, 034619 (2015).
[27] T. Banerjee, S. Nath, A. Jhingan, G. Kaur, R. Dubey, A. Yadav, P. V. Laveen, A. Shamlath, M. Shareef, J. Gehlot, N. Saneesh, E. Prasad, P. Sugathan, and S. Pal, Phys. Rev. C **94**, 044607 (2016).
[28] S. Y. Van Der Werf, Nucl. Instrum. Methods **153**, 221 (1978).
[29] P. D. Shidling, N. M. Badiger, S. Nath, R. Kumar, A. Jhingan, R. P. Singh, P. Sugathan, S. Muralithar, N. Madhavan, A. K. Sinha, S. Pal, S. Kailas, S. Verma, K. Kalita, S. Mandal, R. Singh, B. R. Behera, K. M. Varier, and M. C. Radhakrishna, Phys. Rev. C **74**, 064603 (2006).
[30] S. Nath, J. Gehlot, E. Prasad, J. Sadhukhan, P. D. Shidling, N. Madhavan, S. Muralithar, K. S. Golda, A. Jhingan, T. Varughese, P. V. M. Rao, A. K. Sinha, and S. Pal, Nucl. Phys. A **850**, 22 (2011).
[31] http://www.nndc.bnl.gov/
[32] http://bricc.anu.edu.au/index.php